

1 **Microchannel fabrication on cyclic olefin polymer substrates via** 2 **1064 nm Nd:YAG laser ablation**

3 **Ronán McCann^{a, b, c, d}, Komal Bagga^{a, b, c}, Robert Groarke^{a, b, c}, Apryll Stalcup^{c, e},**

4 **Mercedes Vázquez^{a, c, e, *}, Dermot Brabazon^{a, b, c, d}**

5 ^aAdvanced Processing Technology Research Centre, Dublin City University, Glasnevin, Dublin 9,
6 Ireland

7 ^bSchool of Mechanical and Manufacturing Engineering, Dublin City University, Dublin 9, Ireland

8 ^cIrish Separation Science Cluster, National Centre for Sensor Research, Dublin City University,
9 Dublin 9, Ireland

10 ^dNational Centre for Plasma Science and Technology, Dublin City University, Dublin 9, Ireland

11 ^eSchool of Chemical Sciences, Dublin City University, Dublin 9, Ireland

12 -----
13 ***Corresponding Author:**

14 **Dr. Mercedes Vázquez**

15 School of Chemical Sciences,

16 Dublin City University, Dublin 9, Ireland

17 **Tel: + 353 1 700 7602**

18 **Fax: + 353 1 700 5503**

19 **E-mail: mercedes.vazquez@dcu.ie**

20 -----
21 **Abstract**

22 This paper presents a method for fabrication of microchannels on cyclic olefin polymer films that
23 have application in the field of microfluidics and chemical sensing. Continuous microchannels were
24 fabricated on 188- μ m-thick cyclic olefin polymer substrates using a picosecond pulsed 1064 nm
25 Nd:YAG laser. The effect of laser fluence on the microchannel morphology and dimensions was
26 analysed via scanning electron microscopy and optical profilometry. Single laser passes were found to
27 produce v-shaped microchannels with depths ranging from 12 to 48 μ m and widths from 44 to 154

28 μm . The ablation rate during processing was lower than predicted theoretically. Multiple laser passes
29 were applied to examine the ability for finer control over microchannel morphology with channel
30 depths ranging from 22 μm to 77 μm and channel widths from 59 μm to 155 μm . For up to five repeat
31 passes, acceptable reproducibility was found in the produced microchannel morphology. Infrared
32 spectroscopy revealed that the polymer surface chemistry was not significantly altered via the laser
33 ablation process. These results were compared to other work conducted on cyclic olefin polymers.

34 **Keywords:** Laser ablation; cyclic olefin polymer; microchannel fabrication; Nd:YAG; picosecond;
35 microfluidics

37 1. Introduction

38 Until recently, the typical materials of choice for microfluidic devices and micro-total analysis
39 systems have been glass or polymers such as polymethyl methacrylate (PMMA), polycarbonate (PC),
40 and polydimethylsiloxane (PDMS). These materials have good mechanical properties, allowing for
41 easy processing but often lack good optical transparency in the mid-ultraviolet spectrum (200 – 300
42 nm). Optical transparency in this range is crucial for the optical analysis of many organic compounds
43 such as aromatics, proteins and nucleic acids. Cyclic-olefin polymer (COP) and co-polymer (COC)
44 are an emerging new classes of polymers which have been noted for their low cost, high chemical
45 resistance, biocompatibility and high optical transparency from NIR to mid-UV wavelengths [1].
46 COPs are also recognized for their low water absorption and high mechanical and dimensional
47 stability when in contact with liquids, and as such make extremely suitable platforms for microfluidic
48 devices when compared with previously used alternatives. Owing to these exceptional properties,
49 COP-based devices have been utilised for various applications such as substrates for chromatographic
50 stationary phases [2] and microfluidic devices for the analysis of drugs [3], IR waveguide coatings [4]
51 and as substrates for laser deposited nanomaterials [5].

52 For microfluidic device fabrication, techniques such as xurography [6], micromilling [7], UV-
53 polymerisation [8] and, more recently, 3D printing [9,10] allow for fast and flexible prototyping of

54 devices leading to shorter periods to device optimisation. For large-scale fabrication of devices,
55 techniques such as hot embossing [11] or injection moulding [12] tend to be used due to their cost-
56 effectiveness. However, these lack the ability for rapid prototyping due to the requirement of moulds
57 or negatives to be fabricated. Contrastingly, laser processing provides a fast, repeatable, clean and
58 cost efficient method of microfluidic device manufacturing. The use of laser processing [13,14] and
59 pulsed laser ablation [15] has been demonstrated to be capable of both surface modification and
60 creation of micro- and nanoscale structures on polymer surfaces, along with the incorporation of
61 nanoparticles onto the substrate surface for functionalisation and nanotexturing [16].

62 Neodymium-doped yttrium aluminium garnet (Nd:YAG) lasers are widely used in industry for
63 materials processing [17], however, very few studies have examined the feasibility of using Nd:YAG
64 lasers for the processing of cyclic olefin polymers [6]. Various alternative laser systems, such as ultra-
65 violet and extreme ultra violet laser systems and femtosecond lasers, have been utilized for polymer
66 processing in the past. UV excimer lasers have been used for the processing of optically transparent
67 polymers [18], and specifically COC [19]. The low ablation depth per pulse for COC, which was
68 found to be smaller when compared to PMMA, would allow for the creation of small features
69 although the extent of ablation was seen to be dependent on the norbornene content of the copolymer
70 [20]. However, UV excimer lasers tend to have higher operating cost and lower beam quality when
71 compared to solid-state laser systems. Extreme ultraviolet (EUV) lasers, typically used in
72 microelectronics manufacturing, have also been shown to be capable of nanoscale changes in depth
73 and surface roughness of polymer surfaces due to low penetration depth of EUV radiation [21,22].
74 Despite these advantages, EUV lasers require a vacuum and highly specialised optics for operation
75 and therefore are not well suited for the fabrication of low-cost microfluidic systems.

76 Femtosecond lasers, which interact with materials through non-linear photon absorption, have been
77 demonstrated for the efficient processing of materials transparent to the wavelength of the laser used
78 [15]. For COP processed using a femtosecond titanium sapphire (800 nm) laser, low surface
79 roughness of the processed area was reported [23]. However, some degradation in optical
80 transmission was seen due to a combination of oxidation and dehydrogenation when compared with

81 PMMA or polystyrene (PS) processed under the same conditions. While fast delivery of power by
82 femtosecond lasers allows for efficient processing of materials transparent to the wavelength of the
83 laser, these systems tend to be both more expensive and complicated to maintain than laser processing
84 systems typically used in industry.

85 In this work, we examine the use of an infrared picosecond pulsed Nd:YAG laser for direct-write
86 fabrication of continuous microchannels on the surface of thin COP substrates. The use of multiple
87 laser passes for fine control of dimensions and dimensional uniformity was also examined. Optical
88 profilometry was used for dimensional analysis of the microchannels and scanning electron
89 microscopy was performed to analyse changes in surface morphology. Raman and infrared
90 spectroscopy were performed to examine the effect of laser processing on the surface chemistry.

91 **2. Material and Methods**

92 *2.1 Materials*

93 The substrate material used was ZeonorFilm ZF14-188 (Zeon) cyclic olefin polymer purchased from
94 Ibsidi, Germany, with a thickness of 188 μm . The polymer sheet was cut, cleaned with isopropanol,
95 rinsed with deionised water and dried using compressed clean dry air to ensure the substrate was
96 pristine prior to laser processing.

97 *2.2 Laser processing and substrate fabrication*

98 The direct-write laser system used consisted of a 1064 nm Q-switched, diode-pumped solid-state
99 neodymium-yttrium aluminium garnet laser (BrightSolutions 1064 WEDGE HF), specifications of
100 which are listed in Table 1. A 2D scanning galvanometer (Raylase SS-12) was used to raster the beam
101 in the xy-plane, and a movable z-stage (PI M-404 4PD) was used to control the position of the
102 sample. The laser beam was focussed to a spot size of 140 μm and scanned unidirectionally across the
103 sample at a speed of 1.2 mm/s to form parallel channels separated by 200 μm . The COP films were
104 mechanically fastened to the sample stage for the duration of processing. Further details of the
105 processing parameters are listed in Table 2.

106

107

Table 1. Specifications of the 1064 nm laser processing system.

Wavelength	1064 nm
Maximum Average Output Power	4.5 W
Maximum Pulse Energy	45 mJ
Repetition Rate	7.5 – 100 kHz
Pulse width	0.7 – 5.2 ns
Beam diameter	140 μm

108

109

110

Table 2: Process parameters used during laser processing of COP substrates.

Process Parameter	Single Pass	Multiple Passes
Fluence	0.15 – 0.78 J/cm ²	0.51 J/cm ²
Scan Rate (mm/s)	1.2	1.2
Beam diameter (μm)	140	140
Pulse Width (ps)	750	750
Pulse Repetition Frequency (kHz)	7.5	7.5
No. of passes	1	2 to 10

111

112 2.3 Characterisation

113 Scanning electron microscopy was conducted using an EVO LS15 (Zeiss) with LaB₆ filament,
 114 accelerating voltage of 10 kV, and a beam current intensity of 25 pA. Samples were gold coated using
 115 a ScanCoat Six (Edwards) sputter coater set at a deposition current of 25mA for 80 s, resulting in a
 116 coating thickness of 34 nm.

117 The profile of the microchannels was examined using a VHX-2000 (Keyence) 3D Optical
 118 Microscope. Samples were previously coated with a 68-nm-thick film of gold using the ScanCoat Six

119 sputter coater, which was sufficient to reduce the transmission in the visible range by approximately
120 90% [24] and allow the sample surface to be imaged optically. Images were taken at 0.43 μm
121 increments upwards from the base of the channel at 1000x magnification. For the figures presented
122 hereafter, the error bars relate to a 90% confidence interval of the measured microchannels width and
123 depth.

124 The optical absorbance of the polymer film at the laser wavelength was examined using a Cary 50
125 (Varian) UV-Vis spectrometer. Infrared spectroscopy was performed to examine changes to the
126 substrate surface chemistry as a result of laser processing. Micro-Raman spectroscopy was conducted
127 using a LabRam HR800 (Jobin-Yvon Horiba) system with an Ar^+ 488 nm air-cooled laser and an
128 accumulation time of 20 s. The HR800 was operated in a backscattering configuration with a
129 resolution of 1.1 cm^{-1} . FTIR spectroscopy was performed using a Perkin 100 spectrometer
130 (PerkinElmer) in attenuated total reflectance (ATR) mode. A baseline correction was applied to the
131 FTIR spectra using Origin Pro 9, to allow accurate comparison of relative peak intensities.

132 2.4 Calculation of ablation rate

133 The number of laser pulses, N , incident per unit area in a scanning beam can be estimated from the
134 laser pulse repetition frequency, f , the beam waist, w_0 , and scan rate, v , as follows [25]:

$$135 \quad N = w_0 f / v \quad (1)$$

136 This will then allow determination of the experimental ablation rate, R_m , i.e. the amount of material
137 removed per pulse, which can be estimated as the measured channel depth, d , divided by N :

$$138 \quad R_m = d / N \quad (2)$$

139 For the parameters used in this work, a value of 875 pulses per unit area of a laser pass was calculated
140 from Equation 1. Theoretical ablation rates, R_t , i.e. the expected amount of material removed per
141 pulse, can be calculated using

$$142 \quad R_t = \alpha^{-1} \cdot \ln(F / F_{th}) \quad (3)$$

143 where F and F_{th} are the input and threshold fluences respectively. The “effective optical penetration
144 depth”, α^{-1} , from the *Beer-Lambert law* can be estimated from the slope of the linear fit of a linear-log
145 plot of the ablation depth versus fluence [26]. Predicted microchannel width, W , for an incident
146 fluence of F can be estimated using w_0 and F_{th} [26] whereby

$$147 \quad W^2 = 2w_0^2 \cdot \ln(F/F_{th}) \quad (4)$$

148 This equation assumes that the microchannel widths are equivalent to a single pulse ablation site
149 rather than a scanning beam of multiple pulses. Some variation from the predicted values is expected
150 as a result of the “incubation effect” [26], whereby defects generated by the interaction of multiple
151 laser shots effectively lower the threshold fluence as the number of laser pulses increases. Despite
152 this, this calculation allows insight into the expected variation between single and multiple scanning
153 passes.

154 **3. Results and Discussion**

155 *3.1 Effect of laser fluence*

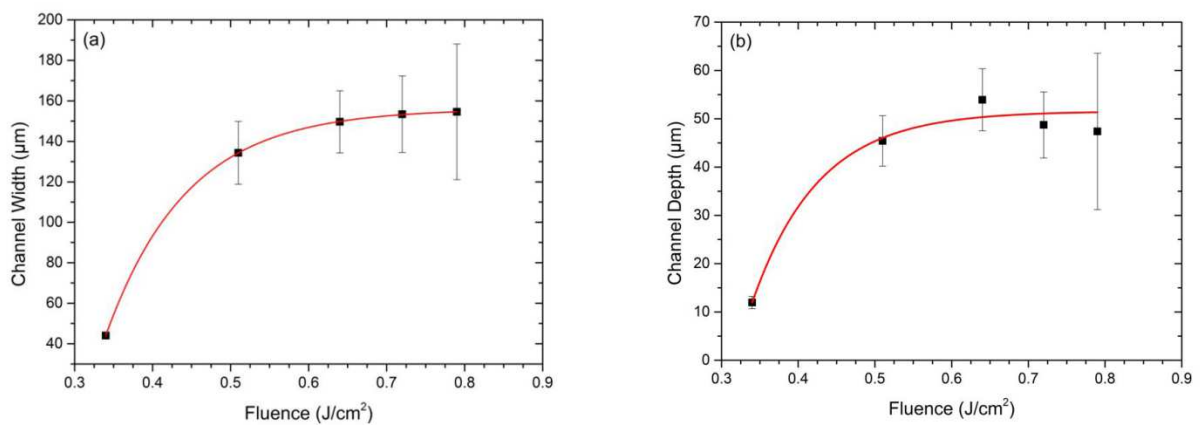
156 The effect of laser fluence on the formation of microchannels on the substrate surface was
157 investigated from the resultant 3D profiles. Both microchannel widths and depths were seen to
158 increase logarithmically with laser fluence as shown in

159 Figure 1. At the lowest fluence used (0.23 J/cm^2), microchannels $44 \text{ }\mu\text{m}$ wide and $12 \text{ }\mu\text{m}$ deep were
160 formed. The highest fluence (0.79 J/cm^2) resulted in microchannels $154 \text{ }\mu\text{m}$ in width and $47 \text{ }\mu\text{m}$ in
161 depth. The logarithmic increase of channel width with increased fluence reflects the underlying
162 absorption mechanism which itself is logarithmically dependant on the ratio between the incident and
163 transmitted laser intensities. A lower correlation coefficient was obtained when a logarithmic fit was
164 applied to the microchannel depth vs. fluence data, indicating there are other factors affecting
165 microchannel depth at high fluences such as energy adsorption and interruption of the chaotic
166 formation of condensed ablated polymer. At all fluences, microchannels with a V-shaped profile were
167 formed, similar to the findings from other work conducted with COP [23], with re-cast ablation melt

168 evident at the channel crests which reduced in size at higher fluences. This reduction may be
169 attributed to thermal diffusion from the ablation site causing a localised melting of condensed debris.
170 For the maximum fluence used (0.79 J/cm^2) heat damage was evident through substrate warping and
171 the appearance of large bubble-like formations on the substrate surface. The increased build-up of
172 heat in the processed area at higher fluences would be expected to result in increased levels of
173 damage. The repetitive and localised nature of this damage followed the pattern of the applied laser
174 pulsing.

175 Figure 2 shows 3D images of the microchannels taken using optical profilometry. For the lower
176 fluence pass (0.34 J/cm^2), a narrow and shallow V-shaped channel with condensed ablated material
177 and melt around the channel edges was observed, see Figure 2a. A wider and deeper microchannel
178 which contained localised deeper ablation sites along the bottom of the channel resulted from the
179 higher fluence pass (0.79 J/cm^2), see Figure 2b.

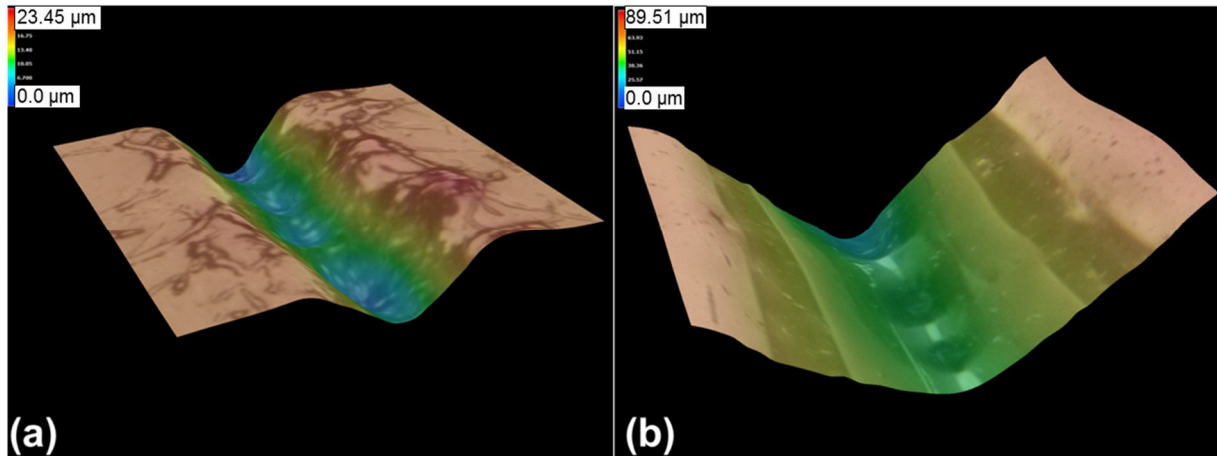
180



181

182 Figure 1. Measured microchannel (a) widths and (b) depths as a function of laser fluence for a single
183 laser pass.

184



185

186 Figure 2. Optical profilometry images of microchannels produced from a single laser pass at a fluence
 187 (a) 0.34 J/cm² and (b) 0.79 J/cm².

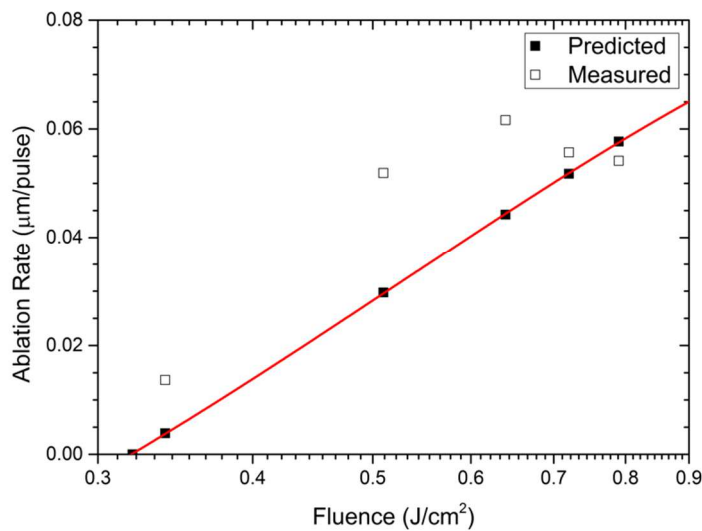
188

189 3.2 Ablation Rate

190 The ablation rate, i.e. the amount of material removed per laser pulse, was calculated to allow for
 191 insight into the laser ablation process under experimental conditions. Figure 3 compares the
 192 experimental ablation rates (Equation 2) and calculated ablation rates (Equation 3). The threshold
 193 fluence (0.32 J/cm²) used in Equation 3, was estimated from the x-axis intercept in Figure 1b. The
 194 effective optical penetration depth, α^{-1} , was determined from the slope of the linear fit applied to
 195 data in Figure 1b once plotted on a linear-log scale, and was found to be 140 nm. For low fluences,
 196 ablation rates of 17 nm/pulse were recorded, while for higher fluences rates of up to 60 nm/pulse were
 197 recorded. These rates were found to be similar to work performed on other grades of cyclic olefin
 198 polymers and copolymers. Ablation rates of approximately 60 – 170 nm/pulse using an ArF excimer
 199 laser [19] and approximately 20 – 70 nm/pulse using a KrF excimer [20] laser have been observed
 200 over a range of laser fluences. The measured ablation rate was seen to plateau after a fluence of 0.64
 201 J/cm².

202 The ablation rate predicted from Equation 1 was higher than that predicted from Equation 3 for
 203 fluences greater than 0.72 J/cm², while for the highest fluence used (0.79 J/cm²) the opposite was

204 found. Equation 1 is based on a theoretical calculation for a single, isolated ablation site. It has been
205 previously discussed that the production of microchannels can result in ablation rates which are higher
206 than expected theoretically due to ablated material being allowed to escape from the previously
207 processed area [25]. Furthermore, as the ablation rate calculation does not incorporate changes in the
208 threshold fluence because of the “incubation effect”, some deviation from the theory is expected.
209 These processes would account for the discrepancy seen in Figure 3 for fluences below 0.79 J/cm².
210 The lower than predicted ablation rate for a fluence of 0.79 J/cm² was attributed to absorption within
211 the laser-generated ablation plume attenuating the laser pulse energy during processing.

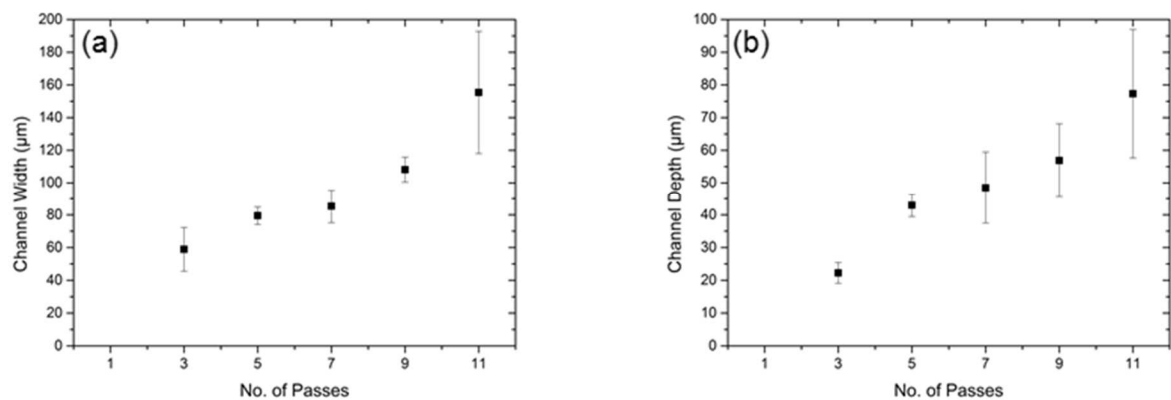


212
213 Figure 3. A comparison of the predicted and measured ablation rates for various laser fluences.

214 3.3 Effect of multiple laser passes

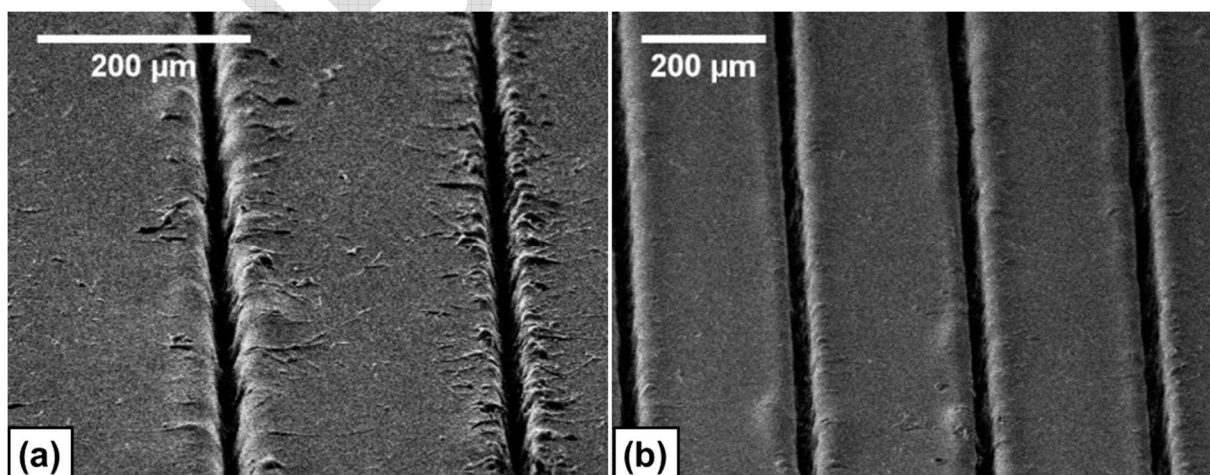
215 Both microchannel width and depth increased with successive laser passes (Figure 4a and 4b
216 respectively). For microchannel depth, there was a noted decrease in channel reproducibility for seven
217 or more passes along with substrate warping during processing. For seven and eleven passes, debris
218 was evident along the channel walls and crests see Figure 5. This debris became more rounded for
219 higher number of laser passes.
220

221 For multiple laser passes, keeping the number of passes at or below five was optimal. This allowed for
222 fine control over the microchannel morphology without a significant decrease in channel
223 reproducibility. This decrease in channel reproducibility above five passes was again attributed to the
224 build-up of heat during processing, as evident by substrate warping, resulting in the substrate surface
225 moving within the laser focal plane. This damage due to build-up of heat at both high fluences and
226 high number of passes highlights the possible need for active cooling of the substrate when high
227 fluence processing is needed. Use of a thicker substrate, which would have a larger thermal mass,
228 could also be a good alternative to minimise this damage.



229

230 Figure 4. Measured microchannel (a) width and (b) depth as a function of number of laser passes.



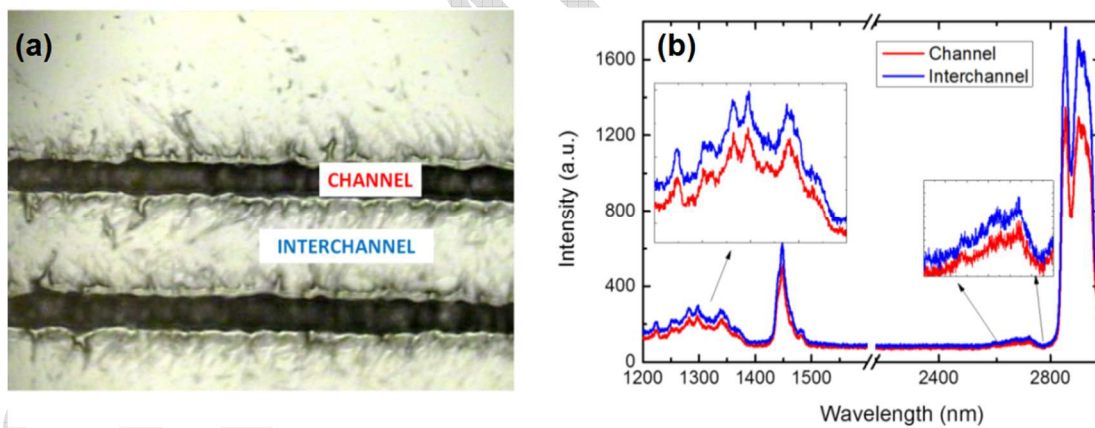
231

232 Figure 5. Scanning electron microscopy images of the COP substrate after (a) 7 and (b) 11 laser
233 passes.

234 3.4 Surface Analysis

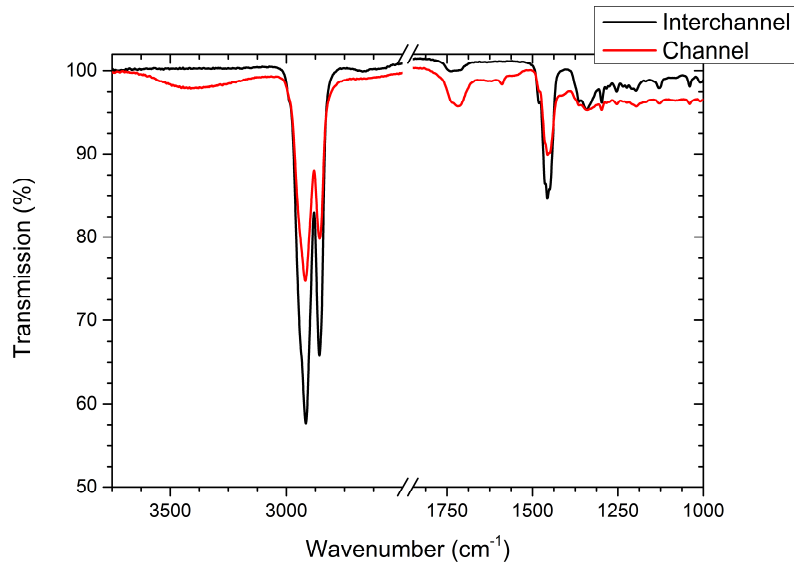
235 Raman and FTIR spectroscopy were performed to study the surface chemical composition after laser
236 processing. The base of the microchannel was examined for changes, while the measurements from
237 the interchannel areas (which were not processed), were used as a reference, as shown in Figure 6a.
238 Both Raman and FTIR (Figure 6b and Figure 7) showed no significant differences in peak position for
239 both the channel and interchannel areas. This indicated that the surface chemistry of the
240 microchannels was not significantly altered by laser processing, thus retaining the chemical resistance
241 and biocompatibility as of the unprocessed COP. Nevertheless, FTIR revealed oxidation after laser
242 processing as evidenced by an increase in IR absorbance at the 1650 – 1750 cm^{-1} range.
243 Dehydrogenation was also evident through a reduction in C-H absorbance at 2800 – 2950 cm^{-1} . The
244 appearance of a broad peak after 3000 cm^{-1} was also observed. These mechanisms of degradation are
245 consistent with that reported for other work on COP [23,27].

246



247

248 Figure 6: Optical image (a) and micro-Raman spectra (b) of the laser processed COP substrates.



249

250 Figure 7: ATR-FTIR spectrum of the COP substrate before and after laser processing.

251 **4. Conclusions**

252 This paper presents the first investigation into laser-texturing of microchannels on cyclic olefin
 253 polymer using an industrial 1064 nm Nd:YAG laser. The ability to tailor microchannel depth and
 254 width by varying laser fluence was demonstrated. Microchannels between 44 μm and 154 μm width
 255 and 12 μm to 47 μm depth were obtained over the fluence range examined. The channels at all
 256 fluences presented a V-shape profile. The experimental ablation rate was calculated based on the
 257 microchannel depth and the number of incident laser pulses, and was compared to that expected from
 258 theory with ablation rates ranging from 13 nm/pulse up to 55 nm/pulse observed.

259 The use of multiple laser passes for fine-tuning of microchannel morphology was also examined with
 260 channel depths ranging from 22 μm to 77 μm and channel widths from 59 μm to 155 μm found. For
 261 up to five repeat laser passes, acceptable reproducibility in channel dimensions was observed allowing
 262 for finer control over channel depths and widths. However, a large decrease in reproducibility of the
 263 microchannel depths occurred for seven passes and above. Both infrared and Raman spectroscopy
 264 revealed that the laser processing had not significantly altered the chemical composition of the
 265 polymer substrate. However, indications of substrate oxidation and dehydrogenation were seen in the
 266 FTIR spectra as expected based on previously reported work on laser processing of cyclic olefin

267 polymers. Ultimately, this work should allow for quick, single-step fabrication of reproducible
268 microchannels on optically transparent substrates that have applications in lab-on-a-chip and
269 microfluidic devices.

270

271 **Acknowledgements**

272 This publication has emanated from research conducted with the financial support of Science
273 Foundation Ireland (SFI) under Grant Number 12/IA/1576 and the European Union's Horizon 2020
274 Research and Innovation Program under the Marie Skłodowska-Curie grant agreement No. 655194.
275 The authors would like to thank Dr. Rajani Vijayaraghavan for assistance with the Raman
276 spectroscopy, and Mr. Vincent Hooper for assistance with the FTIR spectroscopy.

277

278

279

280

281

282

283

284

285

286

287

288

289

291 **References**

- 292 [1] P.S. Nunes, P.D. Ohlsson, O. Ordeig, J.P. Kutter, Cyclic olefin polymers: Emerging materials
293 for lab-on-a-chip applications, *Microfluid. Nanofluidics*. 9 (2010) 145–161.
- 294 [2] K. Faure, M. Albert, V. Dugas, G. Crétier, R. Ferrigno, P. Morin, et al., Development of an
295 acrylate monolith in a cyclo-olefin copolymer microfluidic device for chip
296 electrochromatography separation., *Electrophoresis*. 29 (2008) 4948–55.
- 297 [3] Y. Yang, C. Li, J. Kameoka, K.H. Lee, H.G. Craighead, A polymeric microchip with
298 integrated tips and in situ polymerized monolith for electrospray mass spectrometry., *Lab*
299 *Chip*. 5 (2005) 869–76.
- 300 [4] Y.-W. Shi, Y. Wang, Y. Abe, Y. Matsuura, M. Miyagi, H. Uyama, et al., Fabrication of cyclic
301 olefin polymer (COP)-coated silver hollow glass waveguides for the infrared, in: M.S. Bogner,
302 S.T. Charles, W.S. Grundfest, J.A. Harrington, A. Katzir, L.S. Lome, et al. (Eds.), *Proc. SPIE,*
303 *Surgical-Assist Systems*, San Jose, CA., USA, 1998: pp. 96–102.
- 304 [5] S. Inguva, R.K. Vijayaraghavan, E. McGlynn, J.-P. Mosnier, Highly transparent and
305 reproducible nanocrystalline ZnO and AZO thin films grown by room temperature pulsed-
306 laser deposition on flexible Zeonor plastic substrates, *Mater. Res. Express*. 2 (2015) 096401.
- 307 [6] A. Ben Azouz, S. Murphy, S. Karazi, M. Vázquez, D. Brabazon, Fast Fabrication Process of
308 Microfluidic Devices Based on Cyclic Olefin Copolymer, *Mater. Manuf. Process*. 29 (2014)
309 93–99.
- 310 [7] P.-C. Chen, C.-W. Pan, W.-C. Lee, K.-M. Li, An experimental study of micromilling
311 parameters to manufacture microchannels on a PMMA substrate, *Int. J. Adv. Manuf. Technol.*
312 71 (2014) 1623–1630.
- 313 [8] S. Turri, M. Levi, E. Emilriti, R. Suriano, R. Bongiovanni, Direct Photopolymerisation of
314 PEG-Methacrylate Oligomers for an Easy Prototyping of Microfluidic Structures, *Macromol.*
315 *Chem. Phys*. 211 (2010) 879–887.
- 316 [9] X. Zhang, X. Jiang, C. Sun, Micro-stereolithography of polymeric and ceramic
317 microstructures, *Sensors Actuators A Phys*. 77 (1999) 149–156.
- 318 [10] A.I. Shallan, P. Smejkal, M. Corban, R.M. Guijt, M.C. Breadmore, Cost-effective three-
319 dimensional printing of visibly transparent microchips within minutes., *Anal. Chem*. 86 (2014)
320 3124–30.
- 321 [11] R.K. Jena, C.Y. Yue, Y.C. Lam, Micro fabrication of cyclic olefin copolymer (COC) based
322 microfluidic devices, *Microsyst. Technol*. 18 (2011) 159–166.
- 323 [12] M. Matschuk, H. Bruus, N.B. Larsen, Nanostructures for all-polymer microfluidic systems,
324 *Microelectron. Eng*. 87 (2010) 1379–1382.
- 325 [13] J.-Y. Cheng, C.-W. Wei, K.-H. Hsu, T.-H. Young, Direct-write laser micromachining and
326 universal surface modification of PMMA for device development, *Sensors Actuators B Chem*.
327 99 (2004) 186–196.
- 328 [14] O. Lyutakov, J. Tůma, I. Huttel, V. Prajzler, J. Siegel, V. Švorčík, Polymer surface patterning
329 by laser scanning, *Appl. Phys. B*. 110 (2013) 539–549.
- 330 [15] S. Baudach, J. Bonse, J. Krüger, W. Kautek, J. Kruger, Ultrashort pulse laser ablation of
331 polycarbonate and polymethylmethacrylate, *Appl. Surf. Sci*. 154-155 (2000) 555–560.
- 332 [16] V.N. Bagratashvili, N. V. Minaev, A.A. Rybaltovsky, A.O. Rybaltovsky, S.I. Tsygina, V.Y.

- 333 Panchenko, et al., Laser fabrication of periodic microstructures from silver nanoparticles in
334 polymer films, *Laser Phys.* 20 (2010) 139–143.
- 335 [17] S. Prakash, B. Acherjee, A.S. Kuar, S. Mitra, An experimental investigation on Nd:YAG laser
336 microchanneling on polymethyl methacrylate submerged in water, *Proc. Inst. Mech. Eng. Part*
337 *B J. Eng. Manuf.* 227 (2013) 508–519.
- 338 [18] Y.-T. Chen, K. Naessens, R. Baets, Y.-S. Liao, A.A. Tseng, Ablation of Transparent Materials
339 Using Excimer Lasers for Photonic Applications, *Opt. Rev.* 12 (2005) 427–441.
- 340 [19] D. Sabbert, J. Landsiedel, H.-D. Bauer, W. Ehrfeld, ArF-excimer laser ablation experiments
341 on Cycloolefin Copolymer (COC), *Appl. Surf. Sci.* 150 (1999) 185–189.
- 342 [20] P.W. Leech, Effect of norbornene content on laser ablation of cyclic olefin copolymers,
343 *Mater. Des.* 31 (2010) 4858–4861.
- 344 [21] A. Bartnik, H. Fiedorowicz, R. Jarocki, J. Kostecki, M. Szczurek, O. Chernyayeva, et al.,
345 EUV-induced physico-chemical changes in near-surface layers of polymers, *J. Electron*
346 *Spectros. Relat. Phenomena.* 184 (2011) 270–275.
- 347 [22] Inam Ul Ahad, A. Bartnik, H. Fiedorowicz, J. Kostecki, B. Korczyk, T. Ciach, et al., Surface
348 modification of polymers for biocompatibility via exposure to extreme ultraviolet radiation., *J.*
349 *Biomed. Mater. Res. A.* 102 (2014) 3298–310.
- 350 [23] R. Suriano, A. Kuznetsov, S.M. Eaton, R. Kiyani, G. Cerullo, R. Osellame, et al., Femtosecond
351 laser ablation of polymeric substrates for the fabrication of microfluidic channels, *Appl. Surf.*
352 *Sci.* 257 (2011) 6243–6250.
- 353 [24] O. Loebich, The optical properties of gold, *Gold Bull.* 5 (1972) 2–10.
- 354 [25] A. Rodríguez, A. Arriola, T. Tavera, N. Pérez, S.M. Olaizola, Enhanced depth control of
355 ultrafast laser micromachining of microchannels in soda-lime glass, *Microelectron. Eng.* 98
356 (2012) 672–675.
- 357 [26] A. Ben-Yakar, R.L. Byer, Femtosecond laser ablation properties of borosilicate glass, *J. Appl.*
358 *Phys.* 96 (2004) 5316–5323.
- 359 [27] C. Liu, J. Yu, X. Sun, J. Zhang, J. He, Thermal degradation studies of cyclic olefin
360 copolymers, *Polym. Degrad. Stab.* 81 (2003) 197–205.
- 361